Chemical Science

ROYAL SOCIETY OF CHEMISTRY

EDGE ARTICLE

View Article Online
View Journal | View Issue

Cite this: *Chem. Sci.*, 2022, **13**, 6929

All publication charges for this article have been paid for by the Royal Society of Chemistry

A peptide-derived strategy for specifically targeting the mitochondria and ER of cancer cells: a new approach in fighting cancer†

Yang Sung Sohn, *[a] Anat Iosub-Amir,*[b] Alfredo E. Cardenas, *[c] Ola Karmi,[ad] Merav Darash Yahana,[a] Tal Gruman,[b] Linda Rowland,[d] Henri-Baptiste Marjault,[a] Lauren J. Webb, [e] Ron Mittler, [d] Ron Elber, [c] Assaf Friedler *[b] and Rachel Nechushtai *[a]

Received 4th April 2022
Accepted 18th April 2022

DOI: 10.1039/d2sc01934e

rsc.li/chemical-science

An effective anti-cancer therapy should exclusively target cancer cells and trigger in them a broad spectrum of cell death pathways that will prevent avoidance. Here, we present a new approach in cancer therapy that specifically targets the mitochondria and ER of cancer cells. We developed a peptide derived from the flexible and transmembrane domains of the human protein NAF-1/CISD2. This peptide (NAF-1^{44-67}) specifically permeates through the plasma membranes of human epithelial breast cancer cells, abolishes their mitochondria and ER, and triggers cell death with characteristics of apoptosis, ferroptosis and necroptosis. *In vivo* analysis revealed that the peptide significantly decreases tumor growth in mice carrying xenograft human tumors. Computational simulations of cancer *vs.* normal cell membranes reveal that the specificity of the peptide to cancer cells is due to its selective recognition of their membrane composition. NAF-1^{44-67} represents a promising anti-cancer lead compound that acts *via* a unique mechanism.

Introduction

The mitochondrial-ER network plays a pivotal role in dictating life or death decisions in response to many different environmental and developmental stimuli. Recent studies identified a critical role for the ER, mitochondria and mitochondrial-associated membrane (MAM) network of cancer cells in promoting survival, tumor growth and metastasis.[1,2] One of the proteins localized to the MAM, outer mitochondrial membranes (OMM) and ER is the iron-sulfur cluster [2Fe–2S] protein CISD2 (CDGSH iron-sulfur domain-containing protein 2; also known as nutrient autophagy factor 1; NAF-1).[3,4] NAF-1 plays a key role in regulating calcium, reactive oxygen species (ROS), and iron homeostasis and signalling in cells.[4–9] It also controls several different cell death and recycling pathways including apoptosis, ferroptosis and autophagy.[4,10–13] Elevated levels of NAF-1 expression are associated with the progression of many human cancers and suppressing NAF-1 expression results in reduced cancer proliferation and tumor growth.[5,14] Elevated levels of NAF-1 are also associated with poor prognosis of patients and NAF-1 is used as a diagnostic marker for several different cancers.[5,14–20] NAF-1 is a homodimer, with each subunit containing a *trans*-membrane domain (residues 38–57), a disordered flexible loop (residues 58–67) and a CDGSH [2Fe–2S] soluble binding domain facing the cytosol (resides 68–135).[3] Artificially enhancing NAF-1 expression in cancer cells promoted cellular proliferation, and this promotion was dependent on the degree of lability of the NAF-1 Fe–S clusters.[14] NAF-1 is therefore a central regulator of many cellular processes important for cancer proliferation, and this function of NAF-1 is at least partially dependent on the function of its [2Fe–2S] clusters.[3,18,21,22]

A major challenge in cancer-therapy is to develop molecules that induce cancer cell death but have no cytotoxic effect towards normal cells. Cell Penetrating Peptides (CPP) are promising candidates and well explored.[23,24] CPP are peptides of about ≤30 amino acids able to penetrate the plasma membrane (PM) with an energy dependent (endocytosis) or energy independent (direct permeation) mechanism.[25] They are frequently derived from the membrane translocation machinery, such as

[a]*The Alexander Silberman Institute of Life Science, The Hebrew University of Jerusalem, Edmond J. Safra Campus at Givat Ram, Jerusalem 9190401, Israel. E-mail: rachel@mail.huji.ac.il*

[b]*Institute of Chemistry, The Hebrew University of Jerusalem, Edmond J. Safra Campus at Givat Ram, Jerusalem 9190401, Israel. E-mail: assaf.friedler@mail.huji.ac.il*

[c]*Institute for Computational Engineering and Science and Department of Chemistry, University of Texas at Austin, Austin, Texas 78712, USA*

[d]*Department of Surgery, University of Missouri School of Medicine, Christopher S. Bond Life Sciences Center University of Missouri. 1201 Rollins St, Columbia, MO 65201, USA*

[e]*Department of Chemistry, The University of Texas at Austin, 2506 Speedway STOP A5300, Austin, TX 78712, USA*

† Electronic supplementary information (ESI) available. See https://doi.org/10.1039/d2sc01934e

the TAT peptide that leads the permeation of the HIV Trans Activator Protein.[26] Other sources of CPP are antimicrobial peptides (AMPs).[27] For example, the peptide buforin IIb is an antimicrobial peptide derived from histone H2A that shows significant anticancer activity.[28] The peptide discussed in the present manuscript is derived from a source not considered before. It is a fragment of a transmembrane protein, NAF-1 (NAF-1$^{44\text{-}67}$), containing a hydrophobic N terminal segment, which is embedded in the mitochondrial membrane, and a charged C-terminal part that is found in aqueous solution. Attempts of using CPP against cancer cells face the following challenges: (i) the CPP must be selective towards cancer cells; (ii) it must induce cell death; and (iii) it must survive degradation for a sufficient length of time to have an impact. Other desired properties are the ability of the peptide to induce cell death by itself without additional cargo and its ability to target a vital organelle(s) within cancer cells. To our knowledge, at present, there are no CPP satisfying all these criteria. We illustrate in this manuscript that NAF-1$^{44\text{-}67}$ does. NAF-1$^{44\text{-}67}$ selectively kills cancer cells (IC_{50} values of 12–18 μM), without affecting normal cells. It permeates through the PM of human epithelial breast cancer cells (MDA-MB-231), but not of healthy cells (MCF-10A), and targets their mitochondria and ER. Atomically detailed simulations of the interactions of NAF-1$^{44\text{-}67}$ with models of cancer and normal PM, explain the NAF-1$^{44\text{-}67}$ permeation specificity towards cancer cells. The negatively charged PM of cancer cells strongly attracts the positive charges of NAF-1$^{44\text{-}67}$, while the less negatively charged PM of healthy cells does not. The initial attraction and settling of the peptide at the membrane surface, demonstrated in this paper, is followed by efficient permeation of the transmembrane component of NAF-1$^{44\text{-}67}$ into the membrane core.[29] Upon permeation, the peptide activates several cell death processes that display characteristics of ferroptosis, apoptosis and necroptosis. *In vivo* studies of NAF-1$^{44\text{-}67}$ using xenograft mice carrying human triple-negative breast cancer MDA-MB-231 tumors indicate a significant decrease in tumor growth. The peptide is selective towards cancer cells because it is derived from the NAF-1 sequence that resides in the mitochondrial and ER membranes. It is thus: (i) selective for cancer cells PMs, which resemble the mitochondrial membrane in their composition; and (ii) it specifically targets the mitochondria and ER of cancer cells where NAF-1 normally resides. Taken together, we are presenting a new approach in cancer therapy of targeting of the mitochondria and ER of cancer cells using peptides derived from native proteins of this network.

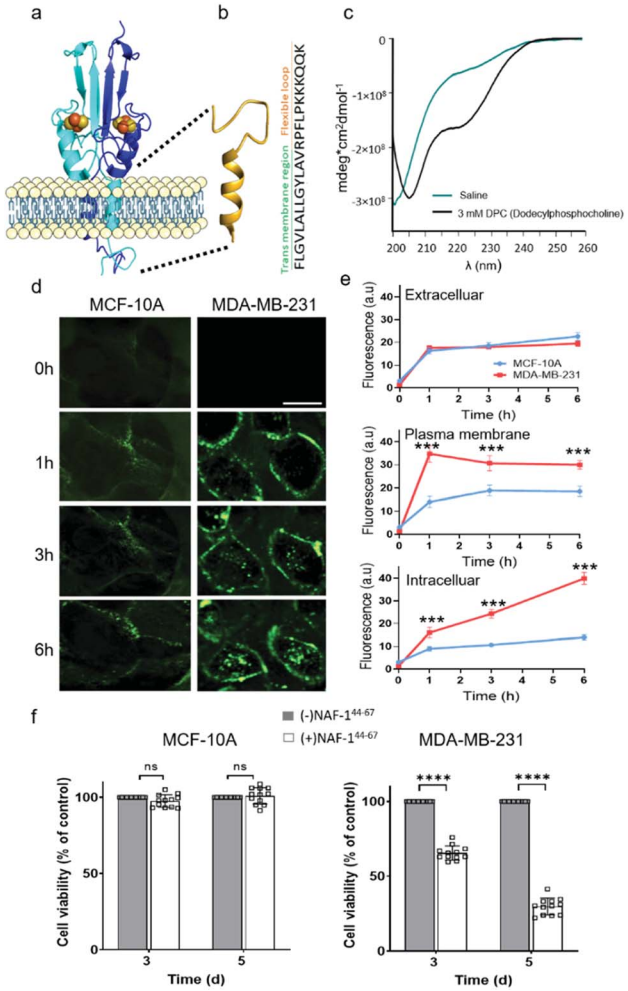

Fig. 1 NAF-1$^{44\text{-}67}$, derived from the transmembrane and flexible loop regions of NAF-1, selectively kills cancer cells. (a) Schematic model of NAF-1 structure (PDB 3FNV). Dashed lines show the NAF-1 region from which the NAF-1$^{44\text{-}67}$ peptide is derived. (b) Predicted structure of NAF-1$^{44\text{-}67}$ showing the transmembrane and flexible regions. (c) The CD spectrum of NAF-1$^{44\text{-}67}$ in saline (turquoise) or 3 mM DPC (black). (d) Confocal fluorescence images of control MCF-10A (left) and MDA-MB-231 breast cancer cells (right) at different time points following treatment with Fl-NAF-1$^{44\text{-}67}$. The scale bar is 20 μm. (e) Quantitative analysis of Fl-NAF-1$^{44\text{-}67}$ penetration into MDA-MB-231 (red lines) or MCF-10A (blue lines) cells. Data is shown as mean ± SD of 25 cells per field calculated for each time-point obtained from $n = 5$ independent experiments. ***$P < 0.001$ by t-test. (f) Cytotoxicity of the NAF-1$^{44\text{-}67}$ peptide towards malignant MDA-MB-231 and control MCF-10A cells. ****$P < 0.0001$ by t-test.

Results

NAF-1$^{44\text{-}67}$ is derived from the transmembrane and flexible loop regions of NAF-1 and forms a helix in a membrane-like environment

NAF-1$^{44\text{-}67}$ is derived from part of the NAF-1 transmembrane helix (residues 44–56) and its disordered loop (residues 57–67; Fig. 1a). The predicted structure of NAF-1$^{44\text{-}67}$ is shown in Fig. 1b. The CD spectrum of the peptide in saline (165 mM NaCl dissociated in water) shows a disordered nature. Whereas in the presence of 3 mM Dodecylphosphocholine (DPC) that form micelles, the CD spectrum of the peptide shifts to a helical structure combined with some disordered features (Fig. 1c).

NAF-1$^{44\text{-}67}$ selectively permeates and kills cancer cells

To study how NAF-1$^{44\text{-}67}$ interacts with cells, we labelled it with fluorescein (Fl-NAF-1$^{44\text{-}67}$) and followed its translocation into triple negative malignant epithelial breast cancer (MDA-MB-231) and non-malignant control (MCF-10A) cells using confocal microscopy. Fl-NAF-1$^{44\text{-}67}$ fluorescence was primarily found outside of control MCF-10A cells, indicating that the

peptide did not permeate normal cells. In contrast, a high Fl-NAF-1^{44-67} fluorescence signal was found at the PM of MDA-MB-231 cancer cells at early stages, and inside MDA-MB-231 cancer cells at 3 and 6 hours of incubation, indicating that Fl-NAF-1^{44-67} preferentially penetrated MDA-MB-231 cancer cells (Fig. 1d, e and S1†). To determine the effect of NAF-1^{44-67} on cancer cells compared to normal healthy cells, we measured the viability of MDA-MB-231 and MCF-10A cells following treatment with 10 μM of NAF-1^{44-67} for three and five days. The viability of MDA-MB-231 cancer cells treated with the peptide decreased by 40% at three days and by 80% at five days post treatment, whereas that of MCF-10A control cells remained unaffected (Fig. 1f). We also tested the penetration and cytotoxic effects of NAF-1^{44-67} on other non-malignant immortalized cells, such as rat cardio myoblast H9C2 cells and human embryonic kidney 293 HEK cells. These cells showed no entry of Fl-NAF-1^{44-67} and remained unaffected after 3 days of treatment (Fig. S2†).

Molecular simulations of NAF-1^{44-67} permeation into cancer cells

Molecular simulations were performed to determine the mechanisms governing the selective entry of NAF-1^{44-67} into cancer cells. The PMs of control and cancer cells were modelled based on lipidomic analysis of control human mammary epithelial breast and MDA-MB-231 breast cancer cell lines.[30] Studies of different cancer cells revealed that the outer layer of their PM is rich with negatively charged PS phospholipids, while the outer layer of a normal PM mostly contains zwitterionic phospholipids.[31–33] Simulating the binding of NAF-1^{44-67} to the two different membranes revealed that, compared to the PM of normal cells, the peptide forms many more electrostatic interactions with the PM of malignant cells (Fig. 2a–c). These interactions were primarily attributed to a higher number of hydrogen bonds formed between NAF-1^{44-67} and the PM of cancer cells (Fig. 2c). Hydrogen bonds can be disrupted by high concentrations of charged ions, such as those present in a solution of $MgCl_2$. We therefore tested the effect of $MgCl_2$ on the binding of NAF-1^{44-67} to membranes *in silico* (Fig. 2c) and *in vivo* (Fig. 2d). Addition of $MgCl_2$ to the molecular simulation revealed that the number of hydrogen bonds formed between NAF-1^{44-67} and the cancer cell PM decreased to that of NAF-1^{44-67} interactions with normal cell PM (Fig. 2c). Addition of $MgCl_2$ to MDA-MB-231 cells incubated with NAF-1^{44-67} revealed that $MgCl_2$ had a strong inhibitory effect on the cancer killing properties of NAF-1^{44-67} (Fig. 2d). Taken together, our findings suggest that formation of hydrogen bonds between NAF-1^{44-67} and the negatively charged PM of cancer cells plays a key role in determining its selectivity and anti-cancer activity. The entire permeation process of NAF-1^{46-67} through a model DOPC membrane was calculated using the method of Milestoning,[84] supporting the picture of strong electrostatic interactions with the membrane surface.

NAF-1^{44-67} targets the mitochondria and ER of cancer cells

Because NAF-1 resides on the cytosolic-facing side of the ER, mitochondrial and MAM membranes, we studied the effects of NAF-1^{44-67} on these organelles within cancer cells. NAF-1^{44-67} caused a loss of mitochondria membrane potential (MMP) and degradation of ER in cancer cells following six hours of incubation. In contrast, the nuclei and PM remained relatively intact, highlighting the specificity of NAF-1^{44-67} to the mitochondria and ER (Fig. 3a and b). In addition, the Fl-NAF-1^{44-67} peptide colocalized to the mitochondria and ER (Fig. S3 and S6†). Transmission electron microscopy (TEM) analysis of MDA-MB-231 cancer cells treated with NAF-1^{44-67} further revealed that NAF-1^{44-67} induced various abnormalities in mitochondria size, cristae integrity and ER structures (Fig. 3c and d); without any apparent effects on the PM and nuclei (Fig. S4†). Mitochondrial functional studies (Fig. S5†) agree with these TEM results. Thus, mitochondrial respiration was significantly decreased, while glycolysis was affected to a much less extent (Fig. S5†).

Taken together, our findings reveal that while NAF-1^{44-67} penetrated the PM of cancer cells (Fig. 1), it did not cause any apparent damage to it, or to the nuclei (Fig. 3 and S6†). Instead, NAF-1^{44-67} primarily damaged the ER and mitochondria of cancer cells (Fig. 3 and S6†). In contrast, NAF-1^{44-67} did not penetrate the PM of normal cells (Fig. 1) and therefore did not damage their content (Fig. 3).

NAF-1^{44-67} induces in cancer cells a cell death process that primarily resembles apoptosis

Proteomics analysis of NAF-1^{44-67}-treated MCF-10A and MDA-MB-231 cells revealed that the expression of several different proteins associated with apoptosis, ferroptosis, necrosis and autophagy was significantly and specifically altered in MDA-MB-231 cells, with the highest proportion of these belonging to apoptotic-like pathways (Fig. 4a. S8, S9 and S10†). Supporting these findings, vesicles resembling apoptotic bodies were also observed in NAF-1^{44-67}-treated MDA-MB-231 cells (Fig. 4b and S7†), and cyclosporine A (CsA), an inhibitor of apoptosis, inhibited NAF-1^{44-67}-induced cell death of MDA-MB-231 spheroids by about 50% (Fig. 4c). In addition, release of cytochrome c from isolated mitochondria (a major hallmark of apoptosis) was observed in isolated mitochondria treated with the NAF-1^{44-67} peptide (Fig. 4d and e). These results suggest that apoptosis, and perhaps other cell death pathways are activated in cancer cells by treatment with NAF-1^{44-67}.

Sequence analysis and development of stable variants of NAF-1^{44-67}

To reveal the minimal sequence required for its activity, we designed four shorter peptides derived from different regions of NAF-1^{44-67}: the transmembrane region (NAF-1^{44-58}; M0; Fig. 5a), part of the transmembrane region and flexible loop (NAF-1^{53-67}; M1; Fig. 5a), the flexible loop (NAF-1^{57-67}; M2; Fig. 5a), and both termini (NAF-$1^{44-52+62-67}$; M3; Fig. 5a). CD spectroscopy revealed that NAF-1^{53-67} and NAF-1^{57-67}, which were mostly derived from the flexible loop, are disordered, whereas NAF-$1^{44-52+62-67}$, derived from both the transmembrane helix and the disordered loop, displayed helical and disordered features (Fig. S11a†). NAF-1^{44-58}, the transmembrane derived peptide, was not soluble. Compared to all its derivatives, the parent NAF-1^{44-67}

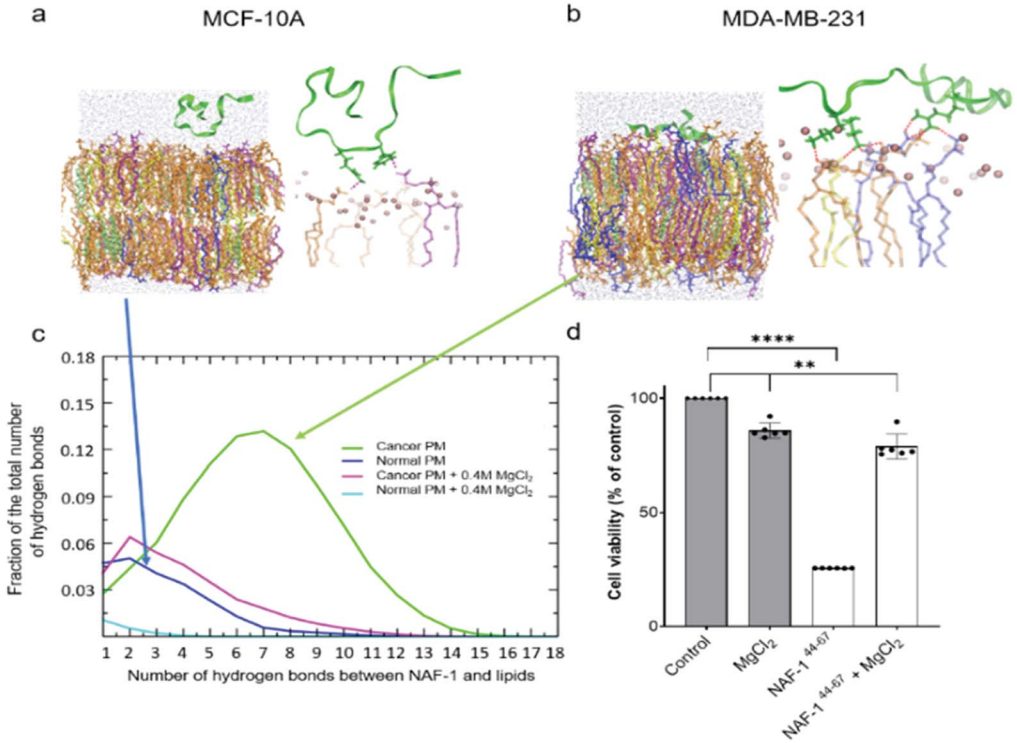

Fig. 2 NAF-$1^{44\text{-}67}$ preferential permeation into epithelial breast cancer cells is dependent on peptide-lipids electrostatic interactions. (a) A molecular simulations snapshot of NAF-$1^{44\text{-}67}$ interaction with the surface of a normal cells' PM and detail view of the molecular snapshot shown for the peptide in the normal PM model. Phosphorus atoms at the membrane/water interface are shown as pink spheres. Side chains of the peptide are added to display the atoms forming hydrogen bonds with the lipids (shown in red). (b) A molecular simulations snapshot illustrating the stronger interaction and early insertion of NAF-$1^{44\text{-}67}$ through the cancer cells' membrane and detail view of the molecular snapshot for the peptide in the cancer PM model. (c) Normalized distribution of the number of hydrogen bonds formed between NAF-$1^{44\text{-}67}$ and the lipid molecules of models cancer and normal cell PMs obtained using MD simulations. Also shown are distributions of hydrogen bonding when $MgCl_2$ is added to the aqueous solution of the normal and cancer plasma membranes. (d) Cell viability measurement of cancer cells treated with NAF-$1^{44\text{-}67}$ for 6 hours in the presence or absence of magnesium chloride ($MgCl_2$). ****$P < 0.0001$, **$P < 0.01$ by t-test. In (a) and (b) the NAF-1 peptide is represented as green ribbons. The lipids are shown using bond representations: PS in blue, PC in orange, PE in yellow, PSM in purple and cholesterol in lime. The oxygen atoms of the water molecules are represented with van der Waals spheres.

peptide exhibited the most potent killing effect towards MDA-MB-231 cells (by more than 50%; Fig. 5b), indicating that the full-length sequence of the peptide is required for its activity. Compared to its different variants, the full-length sequence of NAF-$1^{44\text{-}67}$ also contained more amino acids that could form hydrogen bonds with the PM of cancer cells (Fig. 2b), potentially allowing it to bind better to the cancer cell PM that contains a larger number of negatively charged phospholipids than the PM of a normal cell.

To improve the stability of NAF-$1^{44\text{-}67}$ in biological systems, we incorporated D amino acid residues into its sequence. We synthesized a peptide in which all residues were replaced by D amino acids (D-NAF-$1^{44\text{-}67}$; Fig. 5a and S11b†). In addition, we designed a peptide in which only specific residues were replaced by D amino acids (3D-NAF-$1^{44\text{-}67}$; Fig. 5a and S11b†). For the latter, we used the Prosper server,[34] which predicted that the most probable protease cleavage sites within NAF-$1^{44\text{-}67}$ are Y53, F59, and K63, and replaced these residues with D-amino acids to form the peptide termed 3D-NAF-$1^{44\text{-}67}$ (Fig S11b and c†). In the presences of Trypsin, the L peptide was fully cleaved after 400 min, while the D and 3D peptides showed no cleavage after 24 hours (Fig. S11c†). In the presence of Chymotrypsin, the L peptide was fully cleaved after 100 min, whereas after 540 min only 65% of the 3D peptide and 10% of the D peptide were cleaved (Fig. S11c†). As expected, the CD spectrum of D-NAF-$1^{44\text{-}67}$ was a mirror image of L-NAF-$1^{44\text{-}67}$ and showed a combination of helical features with some disordered domains (Fig. S11b†). The CD spectrum of the 3D-NAF-$1^{44\text{-}67}$ revealed that while the peptide had a larger proportion of disordered features, it kept some of its helical nature (Fig. S11b†). The peptides derived from NAF-$1^{44\text{-}67}$ induced cell death with an IC_{50} value of 18.3 ± 0.4 μM for the L peptide, 12.8 ± 0.2 μM for the D peptide, and 12.5 ± 0.6 μM for the 3D peptide (Fig. S11d†), indicating that the improved stability by the D amino acid residues did not interfere with the cancer killing activity of the peptide.

NAF-$1^{44\text{-}67}$ reduces tumor mass in xenograft mice injected with MDA-MB-231 triple-negative breast cancer cells

In vivo tumor growth assays were performed in compliance with the Hebrew University Authority for biological and biomedical models (NS-17-15262-4). MDA-MB-231 triple-negative human

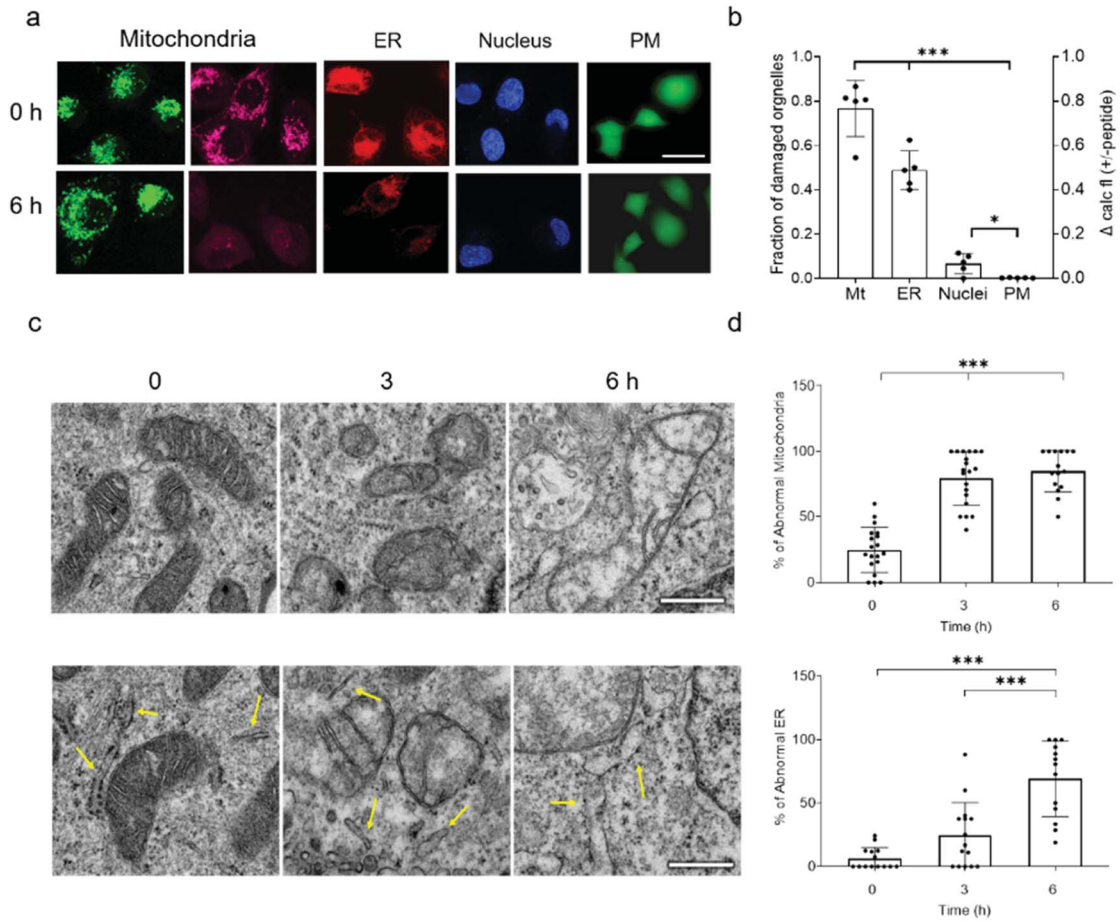

Fig. 3 NAF-1$^{44\text{-}67}$ targets the mitochondria and ER of cancer cells without causing any apparent damage to the PM and nuclei. (a) Representative confocal images of MDA-MB-231 cells incubated with NAF-1$^{44\text{-}67}$. The images were taken at time 0 and after six hours of incubation with the peptide. Cells are stained with MMP-independent mitotracker green or MMP-dependent Rhodamine 800 (mitochondria), DsRed (ER), Hoechst 342 (nuclei), or Calcein AM for testing PM integrity. The scale bar is 20 μm. (b) Degree of damage to the different intracellular structures and PM following six hours of incubation with 10 μM NAF-1$^{44\text{-}67}$. Data is shown as mean ± SD of 75 cells from 15 different fields per time-point, from 5 independent experiments. ***P < 0.001 by t-test. (c) Representative TEM images of structural alterations in mitochondria (top) and ER (bottom) at different time points following incubation with NAF-1$^{44\text{-}67}$. The scale bar is 500 nm. (d) Statistical analysis of structural alterations in mitochondrial (top) and ER (bottom) at different time points following incubation with NAF-1$^{44\text{-}67}$. ***P < 0.001 by t-test. No changes were observed in PM and nuclei structures by TEM (Fig. S4†).

breast cancer cells (3×10^6) were injected subcutaneously to 7 to 8 week-old athymic nude (FOXN1NU) mice. Twenty-eight days after tumor inoculation mice were treated for 3 weeks with either 6 doses of 3D-NAF-1$^{44\text{-}67}$ 50 μM (0.875 mg kg^{-1}) or, as control, with 9 doses of doxorubicin (5 mg kg^{-1}). Treatment of mice with 3D-NAF-1$^{44\text{-}67}$ dramatically reduced tumor growth relative to control untreated mice (Fig. 6a and b). A similar effect of reduction in tumor growth was also found for the potent chemotherapy agent doxorubicin (Fig. 6a and b). However, while doxorubicin treatment caused a severe decrease in body weight during treatment, mice treated with 3D-NAF-1$^{44\text{-}67}$ showed no change in body weight, demonstrating the important non-toxic effect of NAF-1$^{44\text{-}67}$ on mice (Fig. 6c). At the termination of the experiment, tumor weight was measured revealing a significant effect of 3D-NAF-1$^{44\text{-}67}$ on decreasing tumor weight in mice (Fig. 6b). Survival curve assays were performed on younger athymic nude (FOXN1NU) mice, aged 5–6 weeks, that were inoculated subcutaneously with a larger amount (5×10^6) of MDA-MB-231 cells. Rapid tumor growth was established due to the younger age of mice and the higher number of cells inoculated. Mice were treated one week after tumor inoculation for 3 weeks with 6 doses of 3D-NAF-1$^{44\text{-}67}$ peptide 50 μM (0.875 mg kg^{-1}) and a survival curve was established showing a clear mice survival effect on mice treated with the 3D-NAF-1$^{44\text{-}67}$ peptide compared to control saline (Fig. S12†).

Discussion

We describe a peptide, derived from the human NAF-1/CISD2 protein (NAF-1$^{44\text{-}67}$; Fig. 1), which selectively penetrates cancer cells and causes their death without affecting normal cells (Fig. 2), using a unique mechanism. NAF-1$^{44\text{-}67}$ is derived from parts of the transmembrane region and flexible loop of NAF-1 and is mainly helical in DPC. In contrast to many other anticancer peptides that target the PM of cancer cells,[35–39] NAF-1$^{44\text{-}}$

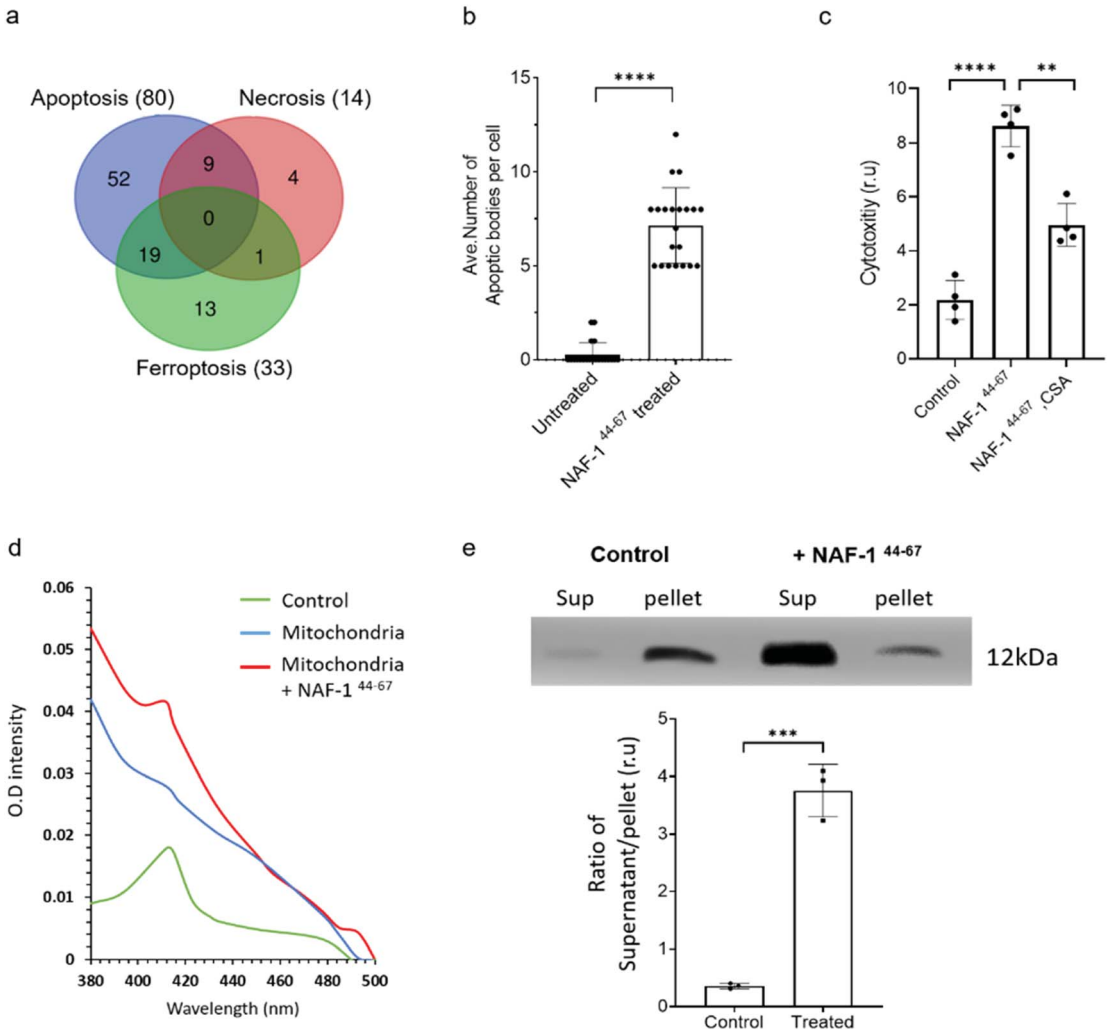

Fig. 4 NAF-1$^{44-67}$ primarily activates apoptosis in cancer cells. (a) Venn diagram showing the overlap between different cell death pathways associated proteins specifically altered in their expression in cancer cells following treatment with NAF-1$^{44-67}$. Most of the proteins (80) affected by the NAF-1$^{44-67}$ peptide belong to the apoptosis cell death pathway. (b) Formation of apoptotic-like bodies (Fig. S7†) in cancer cells following treatment with NAF-1$^{44-67}$. (c) The effect of cyclosporine A, CsA, an inhibitor of apoptosis on the anti-cancer activity of NAF-1$^{44-67}$. MDA-MB-231 spheroids were incubated with NAF-1$^{44-67}$ in the presence or absence of CsA and assayed for cell viability using an IncuCyte apparatus. (d) Isolated mitochondria from MDA-MB-231 breast cancer cells were treated or untreated with NAF-1$^{44-67}$. Mitochondria were precipitated by centrifugation and pellet and soluble fractions collected. The adsorption spectrum with characteristic 420 nm absorption peak of cytochrome C (control) was measured in the supernatant of treated and untreated mitochondria. The absorption of purified cytochrome C (green trace), supernatant of untreated mitochondria (blue trace), and supernatant of mitochondria treated with the NAF-11$^{44-67}$ peptide (red trace). (e) Control and the peptide treated mitochondrial fractions (supernatant, Sup) and pellet, were analysed by western blots with antibodies against cytochrome C [top panel is showing cytochrome C levels in supernatant and pallet from MDA-MB-231 cells treated or nontreated with NAF-1$^{44-67}$; (bottom panel is showing the ratio of Cytochrome C protein levels in supernatant and pellet of control (non-treated) and peptide treated mitochondrial fractions]. The results include all data points measured in three different experiments. $^{**}P < 0.01$, $^{***}P < 0.001$,$^{****}P < 0.0001$ compared to control; Student's *t*-test.

^{67} primarily targets their mitochondria and ER (Fig. 4). Targeting both the mitochondria and ER could be a promising anti-cancer strategy, since the mitochondrial-ER network of cancer cells significantly contributes to the chemoresistance and survival of cancer cells by helping the cancers cells adopt to stress.[40–45]

Peptides with anti-cancer activity targeting mitochondrial proteins and membrane were previously described.[23,29,30] Many of them are chimeric peptides that include a functional sequence that induces apoptosis and a targeting sequence that targets the peptide to the mitochondria.[40,46,47] To the best of our knowledge, NAF-1$^{44-67}$ is the first peptide that selectively penetrates the PM of cancer cells and targets both the ER and the mitochondria (Fig. 4). This behavior of NAF-1$^{44-67}$ is likely a result of the dual targeting of NAF-1 to the ER and mitochondrial membranes in almost all cells studied to date,[10,11] and the similarities observed between the PM of cancer cells and the ER and mitochondrial membranes of healthy cells[48] [Table S1†]. NAF-1$^{44-67}$ could therefore interact with the PM of cancer cells as it would interact with the ER or mitochondrial membranes of

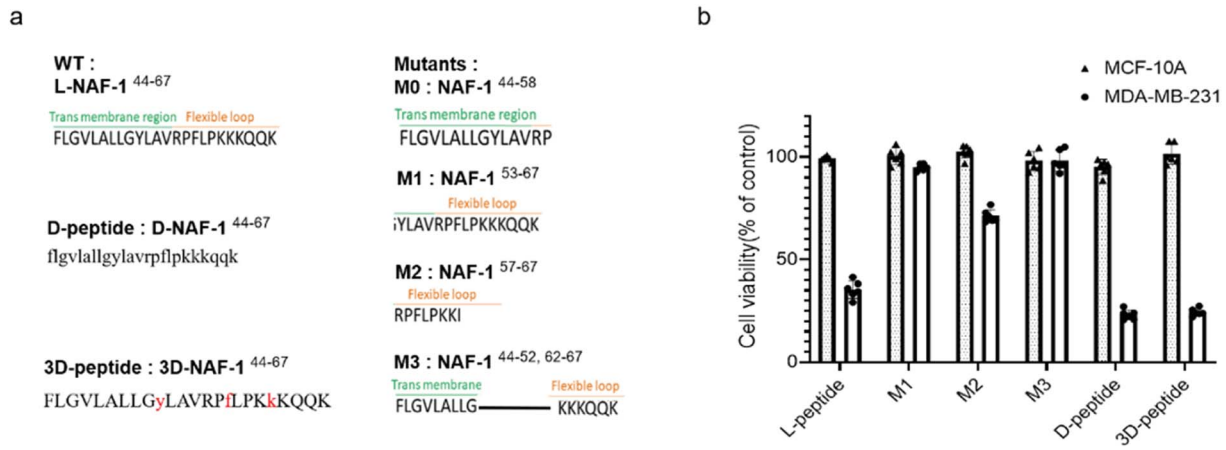

Fig. 5 The full sequence of NAF-1^{44-67} is required for its anti-cancer activity, and NAF-1^{44-67} can be stabilized by incorporating D amino acids. (a) The full sequence of NAF-1^{44-67} and its four mutations, D and 3D peptide sequence. (b) Effect of the NAF-1 derived peptides (10 μM) on the viability of cancer cells (blank, MDA-MB-231) and normal cells (dotted, MCF-10A) after 5 days. L-peptide refers to the original full-length NAF-1^{44-67} peptide.

normal cells, penetrate them without any impact on their integrity, since they do not serve as the target of NAF-1 localization, and continue to interact with and disrupt the cancer cell ER and mitochondrial membranes that are the target of NAF-1 localization. In contrast, since NAF-1^{44-67} does not penetrate the PM of normal cells, that do not resemble ER or mitochondrial membranes of normal cells and do not serve as the target of NAF-1 localization, it does not reach the ER and mitochondrial membranes of normal cells and does not disrupt them.

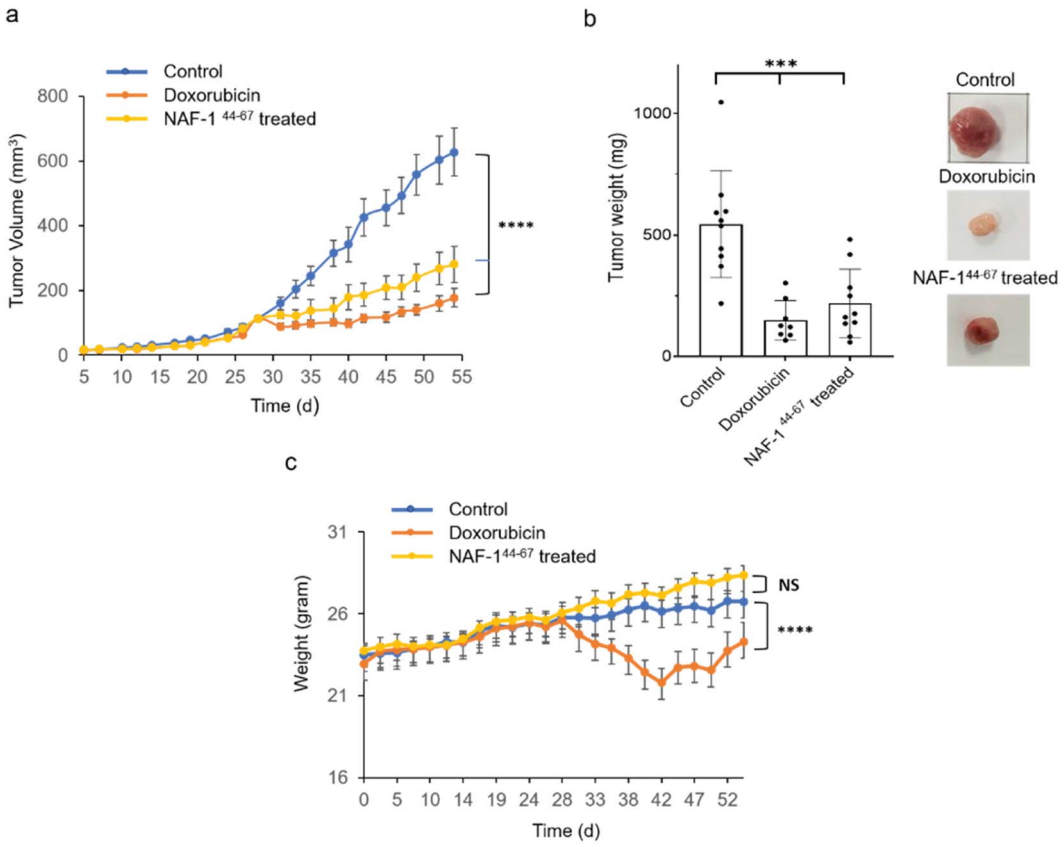

Fig. 6 Treatment with NAF-1^{44-67} reduces tumor size in xenograft mice injected with MDA-MB-231 triple-negative breast cancer cells. (a) The effect of NAF-1^{44-67} or doxorubicin on the volume of MDA-MB-231 tumors developing in xenograft mice. (b) Bar graph (left) and representative images (right) showing the weight and appearance of tumors obtained at termination (week 55) from treated and untreated mice. (c) Changes in body weight of treated and untreated mice. ***$P < 0.001$, ****$P < 0.0001$ by t-test.

Trans-membrane regions of proteins, with or without positively charged amino acids proceeding them, were shown to be responsible for the localization of proteins to their proper organelles, and changing the charge, length or hydrophobicity of this *trans*-membrane region may change protein localization.[49–52] Our simulations show that the *trans*-membrane sequence of NAF-1$^{44\text{-}67}$ is ideal for localizing it to the ER and mitochondrial membranes. The targeting strategy, pursued here, could therefore result in the targeting of the mitochondria and ER of a wide range of cancer cells with very high specificity.

In contrast to other CPP, NAF-1$^{44\text{-}67}$ appears to induce a combination of cell death pathways in cancer cells that primarily includes apoptosis, but also necrosis and ferroptosis, suggesting that NAF-1 could represent a crosstalk point between these different cell death pathways.[53,54] Ferroptosis is a cell death mechanism that is dependent on iron and ROS levels in the cell,[55–58] and NAF-1 regulates the accumulation of ROS and iron in cells.[4] Suppressing NAF-1 in human epithelial breast cancer cells resulted in increased accumulation of Fe and ROS in the mitochondria.[5,14] In addition, suppressing NAF-1 levels resulted in apoptosis and ferroptosis activation in cancer cells.[59,60] The activation of ferroptosis and apoptosis by NAF-1$^{44\text{-}67}$ suggests therefore that this peptide could inhibit the function of the endogenous NAF-1 protein of cancer cells inducing ferroptosis and apoptosis, and that this process may have induced other cell death pathways such as necroptosis.

Taken together, our findings suggest that NAF-1$^{44\text{-}67}$ may induce cancer cell death by two possible mechanisms. The peptide could insert itself into the membranes of the ER and mitochondria, compromising their integrity (that would cause for example leakage of cytochrome c) and activate apoptosis and/or other cell death pathways. Alternatively, or at the same time, the peptide may interfere with the dimerization process of NAF-1, inactivating it and causing activation of different cell death pathways that NAF-1 is protecting cancer cells from (inhibiting the dimerization of a transmembrane region of a protein was shown for example for the receptors ErbB2 and NRP1[61–63]). Because a version of the peptide that contained only D amino acids had a similar killing activity to that of the L amino acid peptide (Fig. 5b), we favour the first mechanism over interfering with dimerization. Regardless of the exact mechanism of cell death initiation, the NAF-1$^{44\text{-}67}$ peptide is unique in the fact that it selectively penetrates through the PM of cancer cells, targeting their mitochondria and ER, and causing cytochrome c release and apoptosis/cell death activation, specifically in cancer cells.

Materials and methods

Peptides synthesis

Peptides were synthesized on a Liberty Blue Microwave Assisted Peptide Synthesizer (CEM) using standard Fmoc chemistry and DIC/Oxyma as coupling reagents. The peptides were labeled with 5(6)-carboxyfluorescein at their N termini as described[64] and cleaved from the resin as described.[65] The peptides were purified on a MERCK-Hitachi HPLC using a reverse-phase C18 semi-preparative column with a gradient of ACN/TDW. ESI mass spectrometry and analytical HPLC were used to verify the identity and purity of the peptides.

Prediction of proteases cleavage sites in the peptides

Prediction of the protease cleavage sites in NAF-1$^{44\text{-}67}$ was performed using PROSPER: PROtease Specificity Prediction servER[34]

Circular dichroism (CD)

CD spectra of different NAF-1$^{44\text{-}67}$ derived peptides were recorded as described.[66] 100 μM peptides were dissolved in 165 mM NaCl (saline) or 3 mM *n*-dodecylphosphocholine (DPC).

Peptide stability against protease cleavage

Peptide stocks of 500 μl in concentrations of 450 μM were added 0.001 mg ml^{-1} protease (trypsin/chymotrypsin) and incubated at 22 °C. Samples of 40 μl were taken before adding the protease and after 15 min, 30 min, 45 min, 1 h, 2 h, 3 h, 4 h, 5 h, 7 h, 9 h and 24 h. 7 μl of 2% TFA in TDW were added to stop the proteolysis. 60 μl TDW were then added and the samples were analyzed using analytical HPLC.

Determination of IC_{50}

MDA-MB-231 cells were planted at a density of 10×10^3 in a 96 well plate and treated with NAF-1$^{44\text{-}67}$ peptides at the series of concentrations (1.25 μM, 2.5 μM, 5 μM, 10 μM, 20 μM, 40 μM, 80 μM, 120 μM, 140 μM, 160 μM) and presto-blue probes (Invitrogen) used for accessing cell death. % of cell death was calculated in reference to cells without the peptide. The IC_{50} values were calculated by fitting the plot to the Hill equation: $Y = B + ((T–B)/(1 + 10(\log^{(EC50)\text{-}X) \times \text{Hill slope}}))$ T and B: top and bottom plateaus in the *Y* axis; EC50: the *X* value that gives the half *Y* value between top and bottom *Y* plateaus. Hill slop is the curve slope.

Cell culture

Malignant epithelial breast cells (MDA-MB-231) were grown in 5% CO_2 RPMI medium 1640 supplemented with 10% FCS, L-glutamine, and antibiotics (Biological Industries). Control epithelial breast cells (MCF-10A) were maintained in complete growth medium consisting of 1 : 1 mixture of Dulbecco's modified Eagle's medium and Ham's F12 medium supplemented with horse serum (5%), epidermal growth factor (20 ng ml^{-1}), cholera toxin (CT, 0.1 μg mg^{-1}), insulin (10 μg ml^{-1}), hydrocortisone (500 ng ml^{-1}), and penicillin/streptomycin (1 unit per ml). Cells were plated one day prior to the experiments on 96-well plates or 4-Chamber Glass Bottom Dish for cell viability or microscopic measurement.[59]

Uptake of fluorescein labelled peptide into cells

Control epithelial breast cells (MCF-10A) and malignant epithelial breast cells (MDA-MB-231) were plated at a density of 2×10^5 cells in 4-Chamber Glass Bottom Dish with 1 ml growth medium and incubated with the Fl-NAF-1$^{44\text{-}67}$ peptide (10 μM) for 24 h.[59] Nuclei were stained with Hoechst 33342 and

mitochondria with Rhodamine 800. Fluorescein fluorescence was observed with a Nikon A1R confocal microscope with GaAsP detectors. Image analysis was conducted using NIS-Elements confocal microscope imaging software.[59]

Cell viability experiments

Cell viability was assayed following incubation of the NAF-1$^{44\text{-}67}$ peptide (10 μM) with MCF-10A or MDA-MB-231 cells plated at a density of 1×10^4 cells per well in 96-well plates. Cells were incubated with the peptide for 3 and 5 days. For the measurement of divalent cations effect, cells were incubated with the peptide in the presence or absence of MgCl2 (0.1 M) following 3 washes (1 ml each) with DMEM-Hepes the cells' viability was determined with the fluorescent redox probe, Presto-Blue.[67] The fluorescence of Presto-Blue was recorded using a plate-reader (Tecan Safire) after 1 h of incubation at 37 °C ($\lambda_{ex} = 560$ nm; $\lambda_{em} = 590$ nm).

Peptide-induced intracellular structure damage assessment

Epithelial breast cells (MCF-10A) and malignant epithelial breast cells (MDA-MB-231) were pre-stained with Rhodamine 800 and Rhodamine B-[(1,10-phenanthrolin-5-yl)-aminocarbonyl] benzyl ester (RPA), for mitochondria, Hoechst 33 342 for nuclei, Calcein-AM for plasma membrane integrity, or modified to stably express pDsRed for ER, and incubated with NAF-1$^{44\text{-}67}$ (10 μM). Cell images were captured with confocal microscope at 0, 1, 3 and 6 h post incubation. Intracellular structure damage was assessed by quantifying the decrease in fluorescence change of each intracellular compartments due to the addition of the peptide. Image analysis was conducted using ImageJ.[14,59]

Evaluation of the cytotoxicity of the spheroids of breast cancer cells

The MDA-MB-231 cells were seeded in a 96 well ULA plate (Corning 7007) at a density of 2000 and allowed to culture for an additional 3 days to form the spheroids. The resulting spheroids were then treated with 10 μM 3D-NAF-1$^{44\text{-}67}$ and cell death inhibitors (2 μM ferrostatin, 1 μM cyclosporine A, 50 μM necrostatin) and the IncuCyte® Red cytotoxicity reagent (Essen Bioscience Cat #4632) to probe the cell death. Cell images were recorded every two hours, and the result in red color, reflecting cell death, was analyzed with the IncuCyte Zoom system (Essen Bioscience).

Transmission electron microscopy (TEM)

Unless otherwise stated, all reagents were purchase from Electron Microscopy Sciences and all specimen preparation was performed at the Electron Microscopy Core Facility, University of Missouri (https://emc.missouri.edu/). Cells were fixed in 2% paraformaldehyde, 2% glutaraldehyde in 100 mM sodium cacodylate buffer pH 7.35. Cells were then rinsed with 100 mM sodium cacodylate buffer, pH 7.35 containing 130 mM sucrose. Secondary fixation was performed using 1% osmium tetroxide (Ted Pella, Inc. Redding, California). Specimens were then incubated at 4 °C for 1 hour, rinsed with cacodylate buffer, followed by rinsing in with distilled water. En bloc staining was performed using 1% aqueous uranyl acetate (4 °C overnight). A graded dehydration series was performed using ethanol at 4 °C, transitioned into acetone, and dehydrated tissues were then infiltrated with Epon resin for 24 hours at room temperature and polymerized at 60 °C overnight. Sections were cut to a thickness of 75 nm using an ultramicrotome (Ultracut UCT, Leica Microsystems, Germany) and a diamond knife (Diatome, Hatfield PA). Images were acquired with a JEOL JEM 1400 transmission electron microscope (JEOL, Peabody, MA) at 80 kV on a Gatan Ultrascan 1000 CCD (Gatan, Inc, Pleasanton, CA) as previously described.[68,69] Results were evaluated from 5–10 different cells randomly selected, every cell was evaluated for their nuclear and general morphology in low magnification. In higher magnification averaged over 20 fields per cell; at least 100–200 mitochondria and 200–300 ER were counted. Mitochondrial and ER damage were expressed as the ratio of damaged organelle to total number of the organelle, in three independent experiments.[9]

Proteomic analysis

Cells (MDA-MB-231 breast cancer epithelial cells and MCF-10A control epithelial cells) were grown to 80% confluency and treated with 10 μM 3D-NAF-1$^{44\text{-}67}$ peptide for (0, 1, 3 and 6 hours). At the different time points cells were sampled and subjected to protein extraction using 0.175 M Tris–HCl, pH 8.8, 5% SDS, 15% glycerol, 0.3 M DTT, as described in.[70] Protein samples were precipitated with 100% of Acetone, washed, resuspended in urea/thiourea buffer (6 M urea, 2 M thiourea, 100 mM ammonium bicarbonate, pH 8.0) and subjected to protein quantification using 660 nm protein assay. An equal amount of protein (40 μg) from each sample was reduced by DTT, alkylated by IAA and digested by LysC/trypsin overnight. Digested peptides were purified by C18 ziptips. All resuspended samples were analyzed by Bruker timsTOF pro DIA-PASEF acquisition mode with a 90 min LC gradient. The spectral library generation and DIA-PASEF data analysis were completed by Spectronaut (v14).

For spectral library generation, 4 μg of purified peptides from each sample were combined and fractionated by high pH reversed-phase peptide fractionation kit according to the manufacturer's protocol (Thermofisher, Waltham, MA). Each of 8 high pH fractions was acquired by 60 min DDA-PASEF[70] and searched against the Uniprot-Human database (UP000005640, 20 381 entries) with the Pulsar algorithm in Spectronaut using the following criteria: spectrum, peptide and protein FDR 1%, min 3 and max 6 best fragments per peptide. A total 97 495 precursors, 78 084 peptides and 8246 protein groups were included in the library. For dia-pasef data analysis: precursor Qvalue (precursor FDR), protein Qvalue (protein FDR) 1%. MS2 area quantification were filtered based on Qvalue and final PG. quantity was cut-off by 30 (1% quantile). A protein was identified in at least 2 samples per group. On average, >6400 proteins were identified in each sample. A total 7431 proteins were identified in all samples. The global sum normalization method was applied.

The statistical analysis included 1- Likelihood Ratio Test (LRT) for MDA-MB-231 cell type to test the effect of treatment in a series of time course; and 2- Likelihood Ratio Test (LRT) for MCF-10A cell type to test the effect of treatment in a series of time course. Significant changes: p value < 0.01. Proteomics data was deposited in the ProteomeXchange Consortium *via* the PRIDE partner repository with the dataset identifier PXD030509.

Animal studies

This study was performed in strict accordance with the NIH guidelines for the care and use of laboratory animals (NIH Publication no. 85-23 Rev. 1985) and was approved by the Hebrew University Animal Care and Use; The Authority for biological and biomedical models (NS-17-15262-4).

In our protocol we used a known human tumor xenograft model for human breast cancer. We injected MDA-MB-231 human breast cancer cells (3×10^6 cells or 5×10^6) subcutaneously to athymic nude (FOXN1NU) at two different age groups 7–8- or 5–6 weeks old mice. Mice weight and tumor size was measured through the experiment. Age groups 5–6 weeks mice were treated one week after tumor inoculation for 3 weeks with 6 doses of NAF-1 peptide 50 μM (17.5 microgram/mouse) and survival curve was established. Age groups 7–8 weeks mice were treated 28 days after tumor inoculation for 3 weeks with either 6 doses of NAF-1 peptide 50 μM (17.5 microgram/mouse) or 9 doses of Doxorubicin (5 mg kg^{-1}). Tumor areas were calculated according to the formula $V = \frac{1}{2}(\text{Length} \times \text{Width}^2)$. At the end of each experiment the animals were euthanized the tumor was remove, weighed, photographed, and preserved in 10% PFA (paraformaldehyde).

Mitochondrial bioenergetics, oxygen consumption rate (OCR), cellular glycolysis and extracellular acidification rate (ECAR)

OCR and ECAR were measured using a Seahorse XFp, Agilent, cell mito-stress analyzer (Agilent Technologies, Inc., Santa Clara, CA, USA) with the XF Cell Mito Stress Kit and XF Glycolysis Stress Kit (Agilent Technologies, Inc., Santa Clara, CA, USA), according to the manufacturer's instructions. MDA-MB-231 cells (40 000) were grown to approximately 80% confluence in complete medium overnight before the experiment. The initial medium was then exchanged with a seahorse-running medium consists of Dulbecco's modified Eagle's medium (DMEM) base without glucose, L-Glutamine 2 mM, sodium pyruvate 1 mM, glucose added to a final concentration of 25 mM, pH adjusted to be 7.3–7.4. Then microplates containing cells were incubated at 37 °C without CO_2 for 1 h before the assay. Plates were then placed into the XFp analyzer. The OCR was calculated after the sequential additions of oligomycin A 1.5 μM, FCCP 0.75 μM, antimycin A/rotenone 1 μM, using an XF Cell Mito Stress Test kit. The ECAR medium initially did not contain glucose, and then measured after the addition of glucose 10 mM, oligomycin A 2 μM and 2-DG 50 mM. Results were expressed as mean ± SD of three independent experiments. All measurements were recorded at set-interval time points. All materials and compounds obtained from Seahorse Bioscience. Calculations of the OCR and the ECAR tests parameters performed according to the manufacturer recommendations, using the equations described in.[71]

The cells were or were not treated with NAF-$1^{44\text{-}67}$ peptide of 20 μM incubated for 3 h before the experiment is taking place of OCR and ECAR.

Mitochondrial fraction isolation

Mitochondria were isolated following the protocol published by Lampl *et al.*[72] or by using the mitochondria isolation kit for cultured cells from abcam (ab110170). Briefly, 30×10^5 cells were collected and washed with pre-cooled PBS 1× twice and centrifuge at 600×g for 5 min at 4 °C. The cell pellet was resuspended into 1 ml of mitochondrial isolation buffer (200 mM sucrose, 10 mM Tris/MOPS, pH 7.4, and 1 mM EGTA/Tris). Then, the cells were broken using a syringe and a 27-gauge $\frac{1}{2}$ inch needle. The cell debris were centrifuged and the supernatant containing the mitochondria crude were collected. The mitochondria crude extract was centrifugated at 10,000×g for 10 min at 4 °C and the pellet containing the enriched mitochondrial fraction was resuspended in mitochondrial isolation buffer at 4 °C.

Measurements of cytochrome C release

5 mg ml^{-1} of isolated mitochondria were incubated with or without 20 μM of NAF-$1^{44\text{-}67}$ peptide for 30 min in isolation buffer. Mitochondrial fractions were then centrifuged for 10 minutes at 10,000×g at 4 °C. The supernatant was then delicately separated from the pellet. 200 μl of the supernatants of the mitochondrial fraction (with and without treatment with NAF-$1^{44\text{-}58}$) were loaded in a quartz cuvette to measure the absorption spectrum. The cytochrome c spectrum was recorded with the Varian Cary 300 Bio UV-visible Spectrophotometer. The optical density of supernatants was recorded against the isolation buffer as a reference from 380 to 500 nm. 0.25 μM of cytochrome C spectrum was also recorded as positive control. The release of cytochrome C from the enriched mitochondrial fraction was also measured by western blot. Similar volume of pellet and supernatant were prepared for western blot using denaturation buffer and the equal volume of solution was loaded and run into SDS-PAGE gel (15% acrylamide). The proteins were transferred to nitrocellulose blots and incubated with antibody against cytochrome C (1/500; ab13575-abcam). Anti-mouse IgG from Jackson ImmunoResearch Laboratories (West Grove, PA) were used as secondary antibodies.

Computer simulations

Model systems. We modeled membranes of normal and cancer plasma membranes based on lipidomic analysis of human mammary epithelial breast and the highly metastatic MDA-MB-231 cancer cell line.[25] Studies of different cancer cells indicate that the outer layer of their plasma membrane is rich on negatively charged PS phospholipids while the outer layer of a normal plasma membrane mostly contain zwitterionic phospholipids.[26] We followed these observations to model simple models of the cancer and plasma membrane that contains

a mixture of phosphatidylcholine (PC), phosphatidylserine (PS), phosphatidylethanolamine (PE), sphingomyelin (SM) and cholesterol with different composition for each membrane (Table S1†). As preparation for future studies we also prepared model membrane systems corresponding to ER and outer mitochondrial membranes using information coming from conventional lipid analysis[72–74] and mass spectroscopy-based lipidomic analysis[75–77] of mammalian cells. The lipidomic analysis provides detailed phospholipid composition but it does not identify the different contributions of the inner and outer layers, or the contributions of the outer and inner mitochondrial membranes. We used the lipidomic information to select the lipid classes and fatty acid tails that are observed with abundance in the membranes of the two organelles. The lipid composition of the model membranes is shown in Table S1.† For the current simulations aiming to study the initial insertion of the peptide we used the composition of the outer layer to model both layers of the bilayer besides lipids of the PC, PE, PS, PI and SM classes, we included two different cardiolipin (CL) lipids (PVCL2, and TLCL2) in the mitochondrial membrane. Cardiolipin is an anionic phospholipid with four alkyl chains that is present only in mitochondria, mostly in its inner membrane, but it is also detected in the external side of the outer membrane.[78] We modelled the ER membrane with a large level of acyl chain mono unsaturation[79]

Bilayer systems preparation. More details of the system preparation and simulations setup can be found in a previous paper[80] and references within it. The CHARMM-GUI Membrane Builder online software was used to generate the four membrane models.[81] The simulation cells were built with the lipid compositions shown in Table S1.† Both the mitochondrial and ER membrane models contain 160 lipid molecules. We added 15 942 and 14 739 water molecules to the mitochondrial and ER membrane models, respectively to fully hydrate the bilayer systems. We also included K^+ ions to neutralize the negative charged membranes, and an additional 150 mM KCl ions. To prepare the models for the normal and cancer plasma membranes a similar procedure was followed. In this case, the number of lipids in the membrane patches was 300 and the number of water molecules was 15 170 (for the cancer plasma membrane) and 15 017 (for the normal plasma membrane).

General setup of molecular dynamics (MD) simulations. All simulations were performed using CHARMM 36 all-atom force field with the MD package GROMACS.[82] The simulation box size was subject to constant number of particles, pressure, and temperature dynamics. Periodic boundary conditions were applied in all directions. A semi-isotropic pressure coupling scheme, in which the x-y dimension is coupled together while the *z* direction is allowed to fluctuate independently, was used with a target pressure of 1.0 bar. Simulations were run at 303 K using a Nosé-Hoover thermostat. The CHARMM TIP3P water model was used for the water molecules. A 2 fs time step was used with the SETTLE algorithm to constrain the water molecules, and the LINCS algorithm to constrain the rest of the bonds involving hydrogen atoms. Full electrostatics were calculated using the particle mesh Ewald (PME) method, with a cut-off of 1.2 nm, and a mesh size of 0.12 nm. For the van der Waals interaction a cut-off of 1.2 nm was used, with the addition of a force switching term so the force smoothly decays to zero from 1.0 to 1.2 nm. A molecular modeling software PEP-FOLD[83] was used to create an initial structure for the peptide. This structure was solvated in a water box, and a MD simulation was run for 20 ns. The final conformation of the peptide was extracted from the simulation and then inserted in the water layer close to the outer layer of the membrane systems built with CHARMM-GUI. After energy minimization using conjugate gradient, the four membrane + peptide systems were pre-equilibrated for 375 ps following the standard procedure employed by CHARMM-GUI Membrane Builder with a gradual decrease of restraints in the lipids. This was followed for a 2 μs simulation run without any restraints for the mitochondrial and ER membrane systems, and 1 μs run for the cancer and normal plasma membranes. The quantification of hydrogen bonds was done with the H-bond analysis tool in GROMACS.

Conclusions

In summary, we present a new approach for anticancer therapy using a unique CPP derived from a protein localized to the mitochondria-ER network ($NAF\text{-}1^{44\text{-}67}$). This CPP interacts with and transverse the PM of cancer cells that have a somewhat similar composition to that of mitochondria and ER membranes and triggers a combination of different cell death pathways, including ferroptosis and apoptosis, regulated by the native protein it is derived from. In contrast, the peptide does not penetrate the PM of healthy cells that do not resemble mitochondria and ER membranes.

Data availability

Proteomics data was deposited in the ProteomeXchange Consortium *via* the PRIDE partner repository with the dataset identifier PXD030509"). We added representative mass spectra to the ESI.† Please find below a special account access info for viewing the data online: Reviewer account details: Username: reviewer_pxd030509@ebi.ac.uk. Password: pLMCoJad.

Author contributions

Conceptualization: RN, AF, RE and RM. Experimental design: RN, AF, RM and RE. Experimental data collection and analysis: Y-SS, A-IA, OK, AEC, MDY, LR, LJW. Computational studies and analysis: AEC, and RE. LJW contributed to experiments on simplified systems. Funding acquisition: RN, AF, RM, LJW and RE. Wrote the manuscript: Y-SS, A-IA, OK, AEC, RN, RE, AF and RM.

Conflicts of interest

The authors declare no conflict of interest.

Acknowledgements

This research was supported by the MINERVA Center for Biohybrid Complex Systems at the Hebrew University and by the

support of the BSF grant number 2020094 to R. N, A. F, L. J. W., and R. E. and the NIH, Grant no. GM 59796 (to R. E.) and GM 111364 (to R. E., L. J. W., R. M.); the Welch Foundation, Grant no. F-1896 (to R. E) and F-1722 (to L. J. W.); and Part of the computations were done using HPC resources from the Texas Advanced Computing Center (TACC) at the University of Texas at Austin. We gratefully acknowledge the use of facilities at the Texas Materials Institute at the University of Texas at Austin.

References

1 H. Kato and H. Nishitoh, *Front. Oncol.*, 2015, **5**, 93.
2 G. Morciano, S. Marchi, C. Morganti, L. Sbano, M. Bittremieux, M. Kerkhofs, M. Corricelli, A. Danese, A. Karkucinska-Wieckowska and M. R. Wieckowski, *Neoplasia*, 2018, **20**, 510–523.
3 A. R. Conlan, H. L. Axelrod, A. E. Cohen, E. C. Abresch, J. Zuris, D. Yee, R. Nechushtai, P. A. Jennings and M. L. Paddock, *J. Mol. Biol.*, 2009, **392**, 143–153.
4 S. Tamir, M. L. Paddock, M. Darash-Yahana-Baram, S. H. Holt, Y. S. Sohn, L. Agranat, D. Michaeli, J. T. Stofleth, C. H. Lipper and F. Morcos, *Biochim. Biophys. Acta, Mol. Cell Res.*, 2015, **1853**, 1294–1315.
5 Y.-S. Sohn, S. Tamir, L. Song, D. Michaeli, I. Matouk, A. R. Conlan, Y. Harir, S. H. Holt, V. Shulaev and M. L. Paddock, *Proc. Natl. Acad. Sci.*, 2013, **110**, 14676–14681.
6 S. Tamir, J. A. Zuris, L. Agranat, C. H. Lipper, A. R. Conlan, D. Michaeli, Y. Harir, M. L. Paddock, R. Mittler and Z. I. Cabantchik, *PLoS One*, 2013, **8**, e61202.
7 C. H. Lipper, M. L. Paddock, J. N. Onuchic, R. Mittler, R. Nechushtai and P. A. Jennings, *PLoS One*, 2015, **10**, e0139699.
8 N. C. Chang, M. Nguyen and G. C. Shore, *Autophagy*, 2012, **8**, 856–857.
9 O. Karmi, Y. S. Sohn, H. B. Marjault, T. Israeli, G. Leibowitz, K. Ioannidis, Y. Nahmias, R. Mittler, I. Z. Cabantchik and R. Nechushtai, *Antioxidants*, 2021, **10**(8), 1160.
10 S. Amr, C. Heisey, M. Zhang, X.-J. Xia, K. H. Shows, K. Ajlouni, A. Pandya, L. S. Satin, H. El-Shanti and R. Shiang, *Am. J. Hum. Genet.*, 2007, **81**, 673–683.
11 Y.-F. Chen, C.-H. Kao, Y.-T. Chen, C.-H. Wang, C.-Y. Wu, C.-Y. Tsai, F.-C. Liu, C.-W. Yang, Y.-H. Wei and M.-T. Hsu, *Genes Dev.*, 2009, **23**, 1183–1194.
12 C.-C. Lin, T.-H. Chiang, W.-J. Chen, Y.-Y. Sun, Y.-H. Lee and M.-S. Lin, *Injury*, 2015, **46**, 2341–2350.
13 N. C. Chang, M. Nguyen, M. Germain and G. C. Shore, *EMBO J.*, 2010, **29**, 606–618.
14 M. Darash-Yahana, Y. Pozniak, M. Lu, Y.-S. Sohn, O. Karmi, S. Tamir, F. Bai, L. Song, P. A. Jennings and E. Pikarsky, *Proc. Natl. Acad. Sci.*, 2016, **113**, 10890–10895.
15 B. Chen, S. Shen, J. Wu, Y. Hua, M. Kuang, S. Li and B. Peng, *Int. J. Clin. Exp. Path.*, 2015, **8**, 13725.
16 L. Wang, F. Ouyang, X. Liu, S. Wu, H.-m. Wu, Y. Xu, B. Wang, J. Zhu, X. Xu and L. Zhang, *Oncotarget*, 2016, **7**, 3791.
17 L. Yang, S. Hong, Y. Wang, Z. He, S. Liang, H. Chen, S. He, S. Wu, L. Song and Y. Chen, *Oncotarget*, 2016, **7**, 22720.
18 Y. Yang, Y.-s. Bai and Q. Wang, *Oncol. Res.*, 2017, **25**, 605.
19 S.-M. Li, C.-H. Chen, Y.-W. Chen, Y.-C. Yen, W.-T. Fang, F.-Y. Tsai, J.-L. Chang, Y.-Y. Shen, S.-F. Huang and C.-P. Chuu, *Sci. Rep.*, 2017, **7**, 1–13.
20 L. Liu, M. Xia, J. Wang, W. Zhang, Y. Zhang and M. He, *Med. Oncol.*, 2014, **31**, 183.
21 W. D. Foulkes, I. E. Smith and J. S. Reis-Filho, *N. Engl. J. Med.*, 2010, **363**, 1938–1948.
22 O. Karmi, Y. S. Sohn, S. I. Zandalinas, L. Rowland, S. King, R. Nechushtai and R. Mittler, *Free Radical Biol. Med.*, 2021, **176**, 92–104.
23 S. Jones, T. Holm, I. Mäger, Ü. Langel and J. Howl, *Chem. Biol.*, 2010, **17**, 735–744.
24 M. Lukanowska, J. Howl and S. Jones, *Biotechnol. J.*, 2013, **8**, 918–930.
25 G. C. Kim, D. H. Cheon and Y. Lee, *Biochim. Biophys. Acta – Proteins Proteom.*, 2021, **1869**(4), 140604.
26 A. D. Frankel and C. O. Pabo, *Cell*, 1988, **55**, 1189–1193.
27 J. K. Boparai and P. K. Sharma, *Protein Pept. Lett.*, 2020, **27**, 4–16.
28 H. S. Lee, C. B. Park, J. M. Kim, S. A. Jang, I. Y. Park, M. S. Kim, J. H. Cho and S. C. Kim, *Cancer Lett.*, 2008, **271**, 47–55.
29 R. Worch, A. Dudek, P. Borkowska and P. Setny, *Int. J. Mol. Sci.*, 2021, **22**, 5301.
30 M. L. Dória, Z. Cotrim, B. Macedo, C. Simões, P. Domingues, L. Helguero and M. R. Domingues, *Breast Cancer Res. Treat.*, 2012, **133**, 635–648.
31 A. C. Alves, D. Ribeiro, C. Nunes and S. Reis, *Biochim. Biophys. Acta - Biomembr.*, 2016, **1858**, 2231–2244.
32 R. Zwaal, P. Comfurius and E. Bevers, *Cell. Mol. Life Sci.*, 2005, **62**, 971–988.
33 S. Riedl, B. Rinner, M. Asslaber, H. Schaider, S. Walzer, A. Novak, K. Lohner and D. Zweytick, *Biochim. Biophys. Acta – Biomembr.*, 2011, **1808**, 2638–2645.
34 J. Song, H. Tan, A. J. Perry, T. Akutsu, G. I. Webb, J. C. Whisstock and R. N. Pike, *PLoS One*, 2012, **7**, e50300.
35 C. Borghouts, C. Kunz and B. Groner, *J. Pept. Sci.*, 2005, **11**, 713–726.
36 J. S. Mader and D. W. Hoskin, *Expert Opin. Invest. Drugs*, 2006, **15**, 933–946.
37 D. W. Hoskin and A. Ramamoorthy, *Biochim. Biophys. Acta – Biomembr.*, 2008, **1778**, 357–375.
38 R. J Boohaker, M. W Lee, P. Vishnubhotla, J. LM Perez and A. R Khaled, *Curr. Med. Chem.*, 2012, **19**, 3794–3804.
39 M. R. Felício, O. N. Silva, S. Gonçalves, N. C. Santos and O. L. Franco, *Front. Chem.*, 2017, **5**, 5.
40 J. E. Constance and C. S. Lim, *Ther. Delivery*, 2012, **3**, 961–979.
41 S. Wen, D. Zhu and P. Huang, *Future Med. Chem.*, 2013, **5**, 53–67.
42 V. Panda, P. Khambat and S. Patil, *Int. J. Clin. Med.*, 2011, **2**(4), 515–529.
43 F. Martinon, *Acta Oncol.*, 2012, **51**, 822–830.
44 T. Avril, E. Vauleon and E. Chevet, *Oncogenesis*, 2017, **6**, e373.
45 H. Urra, E. Dufey, T. Avril, E. Chevet and C. Hetz, *Trends Cancer*, 2016, **2**, 252–262.

46 H. Ellerby, W. Arap, L. Ellerby, R. Kain, R. Andrusiak, G. Rio, S. Krajewski, C. Lombardo, R. Rao and E. Ruoslahti, *Nat. Med.*, 1999, **5**, 1032–1038.
47 S. Farsinejad, Z. Gheisary, S. E. Samani and A. M. Alizadeh, *Tumor Biol.*, 2015, **36**, 5715–5725.
48 D. Casares, P. V. Escribá and C. A. Rosselló, *Int. J. Mol. Sci.*, 2019, **20**, 2167.
49 M. Nguyen, D. Millar, V. W. Yong, S. Korsmeyer and G. Shore, *J. Biol. Chem.*, 1993, **268**, 25265–25268.
50 I. Arnold, H. Fölsch, W. Neupert and R. A. Stuart, *J. Biol. Chem.*, 1998, **273**, 1469–1476.
51 N. Borgese, S. Colombo and E. Pedrazzini, *Int. J. Cell Biol.*, 2003, **161**, 1013–1019.
52 D. M. Walther and D. Rapaport, *Biochimica et Biophysica Acta – Molecular Cell Research is Biochim. Biophys. Acta*, 2009, **1793**, 42–51.
53 T. Vanden Berghe, W. J. Kaiser, M. J. Bertrand and P. Vandenabeele, *Mol. Cell. Oncol.*, 2015, **2**, e975093.
54 S. H. Hong, D.-H. Lee, Y.-S. Lee, M. J. Jo, Y. A. Jeong, W. T. Kwon, H. A. Choudry, D. L. Bartlett and Y. J. Lee, *Oncotarget*, 2017, **8**, 115164.
55 Y. Xie, W. Hou, X. Song, Y. Yu, J. Huang, X. Sun, R. Kang and D. Tang, *Cell Death Differ.*, 2016, **23**, 369–379.
56 H. Yu, P. Guo, X. Xie, Y. Wang and G. Chen, *J. Cell. Mol. Med.*, 2017, **21**, 648–657.
57 A. R. Bogdan, M. Miyazawa, K. Hashimoto and Y. Tsuji, *Trends Biochem. Sci.*, 2016, **41**, 274–286.
58 W. S. Yang and B. R. Stockwell, *Trends Cell Biol.*, 2016, **26**, 165–176.
59 S. H. Holt, M. Darash-Yahana, Y. S. Sohn, L. Song, O. Karmi, S. Tamir, D. Michaeli, Y. Luo, M. L. Paddock and P. A. Jennings, *J. Cell Sci.*, 2016, **129**, 155–165.
60 S. D. King, C. F. Gray, L. Song, R. Mittler and P. A. Padilla, *PLoS One*, 2021, **16**, e0245174.
61 A. Arpel, P. Sawma, C. Spenlé, J. Fritz, L. Meyer, N. Garnier, I. Velázquez-Quesada, T. Hussenet, S. Aci-Sèche and N. Baumlin, *Cell Rep.*, 2014, **8**, 1714–1721.
62 A. Bennasroune, M. Fickova, A. Gardin, S. Dirrig-Grosch, D. Aunis, G. Crémel and P. Hubert, *Mol. Biol. Cell*, 2004, **15**, 3464–3474.
63 C. Nasarre, M. Roth, L. Jacob, L. Roth, E. Koncina, A. Thien, G. Labourdette, P. Poulet, P. Hubert and G. Crémel, *Oncogene*, 2010, **29**, 2381–2392.
64 P. J. Weber, J. E. Bader, G. Folkers and A. G. Beck-Sickinger, *Bioorg. Med. Chem. Lett.*, 1998, **8**, 597–600.
65 R. Gabizon, M. Mor, M. M. Rosenberg, L. Britan, Z. Hayouka, M. Kotler, D. E. Shalev and A. Friedler, *Pept. Sci.*, 2008, **90**, 105–116.
66 A. I. Amir, M. van Rosmalen, G. Mayer, M. Lebendiker, T. Danieli and A. Friedler, *Sci. Rep.*, 2015, **5**, 1–11.
67 M. Sonnaert, I. Papantoniou, F. P. Luyten and J. Schrooten, *Tissue Eng. – C: Methods*, 2015, **21**, 519–529.
68 X. Pan, S. A. Sands, Y. Yue, K. Zhang, S. M. LeVine and D. Duan, *Hum. Gene Ther.*, 2019, **30**, 1039–1051.
69 S. I. Zandalinas, L. Song, S. Sengupta, S. A. McInturf, D. G. Grant, H. B. Marjault, N. A. Castro-Guerrero, D. Burks, R. K. Azad and D. G. Mendoza-Cozatl, *Plant J.*, 2020, **101**, 1152–1169.
70 B. Yang, R. Li, P. N. Liu, X. Geng, B. P. Mooney, C. Chen, J. Cheng, K. L. Fritsche, D. Q. Beversdorf and J. C. Lee, *J. Proteome Res.*, 2020, **19**, 2236–2246.
71 A. S. Divakaruni, A. Paradyse, D. A. Ferrick, A. N. Murphy and M. Jastroch, *Methods Enzymol.*, 2014, **547**, 309–354.
72 S. E. Horvath and G. Daum, *Prog. Lipid Res.*, 2013, **52**, 590–614.
73 L. Brignac-Huber, J. R. Reed and W. L. Backes, *Mol. Pharmacol.*, 2011, **79**, 549–557.
74 F. Zambrano, S. Fleischer and B. Fleischer, *Biochim Biophys Acta Mol Cell Biol Lipids.*, 1975, **380**, 357–369.
75 S. S. Bird, V. R. Marur, I. G. Stavrovskaya and B. S. Kristal, *Metabolomics*, 2013, **9**, 67–83.
76 A. Y. Andreyev, E. Fahy, Z. Guan, S. Kelly, X. Li, J. G. McDonald, S. Milne, D. Myers, H. Park and A. Ryan, *J. Lipid Res.*, 2010, **51**, 2785–2797.
77 S. Hofmann, M. Krajewski, C. Scherer, V. Scholz, V. Mordhorst, P. Truschow, A. Schöbel, R. Reimer, D. Schwudke and E. Herker, *Biochim. Biophys. Acta – Mol. Cell Biol. Lipids*, 2018, **1863**, 1041–1056.
78 R. Hovius, J. Thijssen, P. van der Linden, K. Nicolay and B. de Kruijff, *FEBS Lett.*, 1993, **330**, 71–76.
79 B. Antonny, S. Vanni, H. Shindou and T. Ferreira, *Trends Cell Biol.*, 2015, **25**, 427–436.
80 M. L. Valentine, A. E. Cardenas, R. Elber and C. R. Baiz, *Biophys. J.*, 2018, **115**, 1541–1551.
81 E. L. Wu, X. Cheng, S. Jo, H. Rui, K. C. Song, E. M. Dávila-Contreras, Y. Qi, J. Lee, V. Monje-Galvan, R. M. Venable, J. B Klauda and W. Im, *J. Comput. Chem.*, 2014, **35**(27), 1997–2004.
82 M. J. Abraham, T. Murtola, R. Schulz, S. Páll, J. C. Smith, B. Hess and E. Lindahl, *SoftwareX*, 2015, **1**, 19–25.
83 Y. Shen, J. Maupetit, P. Derreumaux and P. Tufféry, *J. Chem. Theory Comput.*, 2014, **10**, 4745–4758.
84 A. E. Cardenas, C. I. Drexler, R. Nechushtai, R. Mittler, A. Friedler, L. J. Webb and R. Elber, *J. Phys. Chem. B*, 2022, **126**, 2834–2849.